UNIVERSITY OF CALIFORNIA,
IRVINE

Mechanistic Studies of Organozinc Reagent Formation using Single-Particle Fluorescence Microscopy

THESIS

submitted in partial satisfaction of the requirements
for the degree of

MASTER OF SCIENCE

in Chemistry

by

Tristen Kazumasa Soriano Tagawa

Members of the Thesis Committee:
Professor Suzanne A. Blum, Chair
Professor Vy M. Dong
Associate Dean, Professor David Van Vranken

2021

Table of Contents

List of Figures

I. Introduction

II. Single-Particle Studies of Organozinc Reagent Synthesis with Various Lithium Salts

III. Explaining the High Reactivity of Rieke Zinc

Acknowledgements

I would like to send my greatest appreciation to my advisor, Professor Suzanne A. Blum, for leading my growth as a chemist and fostering a work environment of teamwork, safety, and diligence.

In addition, I would like to thank my committee members, Professor Vy M. Dong and Professor David Van Vranken, for their continued support and guidance for completing this thesis.

I would also like to thank various faculty members at UCI for instrumental assistance: Director Philip R. Dennison for the use of the NMR facility, Director Dmitry Fishman for use of the Laser Spectroscopy Facility, and Professor Zhibin Guan for use of their Karl Fisher Titrator.

I am also grateful for Kristof Jess and Kazuhiro Kitagawa, the coauthors for section II of this thesis. The text in Section II is a reprint of the material as it appears in the *Journal of the American Chemical Society*. The co-authors listed in this publication directed and supervised research which forms the basis for this section of the thesis.

With regards to funding, I would like to thank the National Science Foundation and the University of California, Irvine (UCI). I thank the Journal of the American Chemical Society for permission to include section II of this thesis.

Abstract of the Thesis

Mechanistic Studies of Organozinc Reagent Formation using Single-Particle Fluorescence Microscopy

by

Tristen Kazumasa Soriano Tagawa

Master of Science in Chemistry

University of California, Irvine, 2021

Professor Suzanne A. Blum, Chair

Organozinc reagents are important tools for synthesis due to their highly nucleophilic nature and their ability to participate in transmetalation reactions, such as in Negishi coupling. Various methods for preparation of these compounds have been published, but the mechanisms of these published synthetic routes still remain poorly understood. This thesis will focus on two published methods for organozinc preparation and will document how fluorescence microscopy can be used to investigate these syntheses in ways that cannot be elucidated by traditional analytical tools.

One method of organozinc preparation involves the use of lithium salts, which can promote the direct insertion of metallic zinc powder into an organohalide. Through a combined approach of single-metal-particle fluorescence microscopy with ^{1}H NMR spectroscopy, it was found that the effectiveness of different lithium salts toward solubilizing zinc-surface intermediates establishes a previously unknown reactivity correlation that predicts the propensity of that salt to promote macroscale reagent synthesis and also predicts the solution structure of the ultimate organozinc reagent. This work unifies previously disparate observations under a single unified mechanistic framework.

Another method of organozinc preparation involves the formation of an activated form of Zn (0) by the reduction of $ZnCl_2$ with lithium naphthalenide, which coincidentally leaves behind a LiCl byproduct. This activated zinc could then be added to an organohalide, directly forming the corresponding organozinc. Our initial hypothesis speculated that this LiCl byproduct was effective at rapidly solubilizing organozinc reagent off of the zinc surface. Whereas, salts that are known to be ineffective at solubilization, such as NaCl, should not result in organozinc reagent being released off of the surface. This was investigated by imaging these activated zinc particles on a fluorescence microscope and by modifying the preparative procedure to form these zinc particles with different salt byproducts (i.e., LiCl and NaCl). Both images of the Zn*•2LiCl and Zn*•2NaCl showed absence of the oxidative addition intermediate which suggests that the rapid solubilization step may depend on factors beside the salt byproduct.

Surface-bound reaction intermediates could not be possibly detected without an analysis method with astronomically low levels of detectability. Fluorescence microscopy is this novel method of instrumental analysis due to its high sensitivity and excellent spatiotemporal resolution.

I. Introduction

Organometallic compounds are important reagents in a broad range of syntheses. The nucleophilic nature of the carbon-metal bond allows for a wide variety of applications in synthesis. Organomagnesium (Grignard reagents) are some of the most powerful and oldest tools in synthesis.[1] However, expanding the organometallic toolbox beyond magnesium proves more difficult with more conditions. For example, Knochel found that LiCl significantly enhances the rate of direct insertion of the zinc metal in organohalides (Figure 1, top schematic).[2] This method of forming organometallics was then expanded to indium,[3] manganese,[4] and aluminum[5] using lithium chloride and a multitude of other transition metal additives.[6] Expansion of the organometallic toolbox allows for facile synthesis using a variety of methods, such as using organozinc reagents as transmetalation partners for Negishi cross-coupling reactions.[7] However, the mechanistic role of the additives required in forming these organometallic reagents was, until recently,[8] unknown. Determining the mechanistic role of the additive would give further insight into the salt effects in promoting oxidative addition with other metallic elements. While LiCl was found to favorably alter reactivity of the organometallic reagents,[6] other salts, with the exception of LiBr, have been reported to replicate the same effect.[9,10]

While salt additives like LiCl were found to directly increase the yield of organometallic reagents,[2–6] alternative methods have been found to increase organometallic formation by means of an activated form of the metal, without the need for an additive.[11–13] Rieke discovered that forming zinc (0) by a reduction of $ZnCl_2$ with lithium naphthalenide results in a finely divided zinc powder with a high surface area.[14] This activated form of zinc is extremely reactive and could be utilized to form organozinc reagents directly from the corresponding organohalide (Figure 1, bottom schematic).[13–16] This method was also used prior to this study to form activated magnesium

as well.[14,17–21] In some cases, this magnesium could be used in organomagnesium reactions that were not possible with normal Grignard reagents, such as a 1-choloronorbornane.[22] However, the role of the Rieke metals in expediting organometallic formation remains poorly understood. There are many proposed hypotheses such as the high surface area of the metal particles or the lack of an oxide layer found on the surface.[17,23] However, our current hypothesis for this phenomenon is a direct result of our finding with LiCl in our previous studies on zinc,[24–26] where LiCl remains embedded within the zinc metal in the formation of Rieke zinc,. This LiCl exists amorphously with the solid zinc[17,27,28] and may possibly act as an agent for solubilization of the organozinc product from the zinc surface.

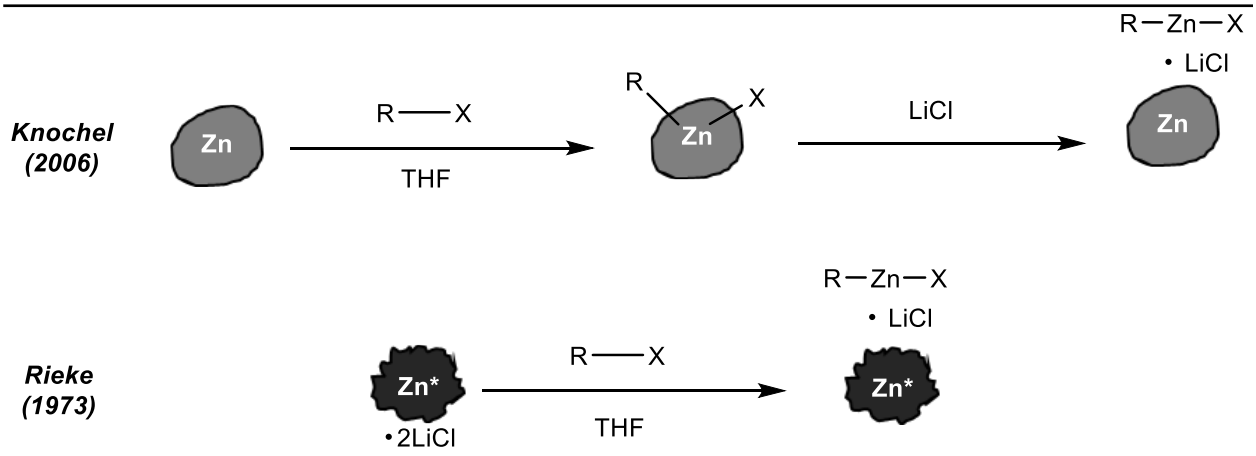

Figure 1. Synthetic methods of forming organozinc reagents.

With traditional analytical techniques, solid-phase reaction intermediates in heterogeneous reactions cannot be properly resolved in a reaction. Fluorescence microscopy allows us to gauge information about the behavior of these intermediates due to the high sensitivity of the technique.[29–36] Using a combined single-metal-particle microscopy technique with an ^{1}H NMR spectroscopy approach, we discover that different salts affect the solubilization of zinc surface intermediates and can predict both the effect on rate acceleration in macroscale synthesis and the solution structure of the organozinc reagent. This new synthetic knowledge provides theoretical

framework that unifies the understanding of previously disparate multiple steps of the salt-mediated syntheses of organozinc reagents, making the effect of lithium salts on multiple steps predictable under one model.

As a current work in progress, fluorescence microscopy can be used to resolve surface intermediates on Rieke zinc to determine the defining characteristic of the activated metal that facilitates facile organozinc formation. The formation of Rieke zinc can be configured to change the alkali salt embedded within the metal, therefore, previously tested salts that fail to solubilize organozinc product (such as NaCl) can be used to prepare Rieke zinc and hypothetically should show surface intermediates if analyzed by fluorescence microscopy.

II. Single-Particle Studies of Organozinc Reagent Synthesis with Various Lithium Salts

A previous study by Feng[30] revealed that oxidative addition intermediates in organozinc synthesis are observable by fluorescence microscopy with high sensitivity (Figure 2). The same method for organozinc synthesis was utilized in this study to observe the effect of various lithium salts. In this experimental design, imaging agent **1** is used as a probe for oxidative addition reactivity on the surface of zinc particles. The imaging agent is composed of a BODIPY (boron dipyrromethene) spectator core, a reactive carbon–iodide bond for oxidative addition, and a butyl chain separating the BODIPY unit from the carbon–iodide site. Due to oxidative addition of **1**, the fluorophore accumulates on the zinc surface when left to react, leading to bright fluorescent hotspots on the zinc surface that represent oxidative addition intermediate **2** bound to the zinc surface. It is not yet clear whether the alkyl group and the iodide are bonded to a common zinc atom. After the addition of lithium salt, microscopy images will show either a persistence or a

disappearance of the fluorescent hotspots, depending on the ability of the salt to solubilize the intermediate into the organozinc solution species **3**.

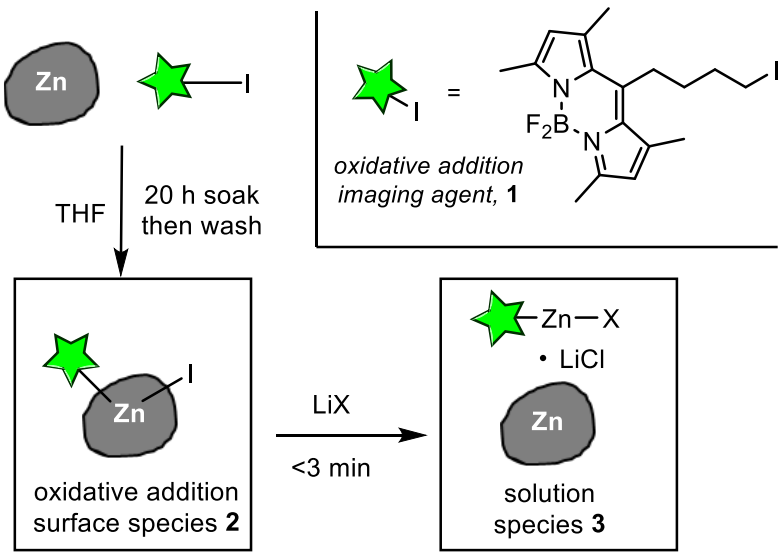

Figure 2. Schematic of the fluorescence microscopy experiments for mechanistic study of Knochel synthesis of organozinc reagents. Inset: Imaging agent for oxidative addition.

In a collaborative study with Jess,[26] we had examined the effects of various conditions in organozinc synthesis using a combined fluorescence microscopy–^{1}H NMR spectroscopy approach. My role in this study was to run the organozinc syntheses with LiF, LiCl, LiBr, and LiI and to examine the zinc particles after alkyliodide addition by fluorescence microscopy, before and after addition of the lithium salt. In the case of LiCl, LiBr, and LiI, fluorescent hotspots had either completely disappeared or significantly dimmed 90-150 s after addition of salt, showing that these salts were effective at solubilizing organozinc product. These results had mirrored the studies with LiCl by Feng.[8,30] In contrast, microscopy showed very little difference in fluorescence before and after the addition of LiF, revealing that LiF is a poor salt at solubilizing the organozinc product. The presence and then absence of oxidative addition intermediate is a phenomenon that has only been visualized by our single-particle microscopy technique.

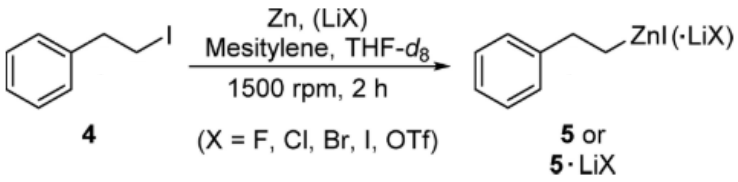

Figure 3. Reaction scheme for ^{1}H NMR spectroscopy experiments. X = OTf was done by Kristof Jess.

To investigate the trend observed by fluorescence microscopy, we studied the conversion of (2-iodoethyl)benzene (**4**) to its corresponding organozinc species **5** by ^{1}H NMR spectroscopy. My role in this section of the study was to generate organozinc reagents with various salts LiX (X = F, Cl, Br, I) and a control experiment with no salt additive present (Figure 3). Jess had completed the experiments with X = OTf. Substrate **4** was reacted with 1.4 equiv of zinc powder and 1 equiv of LiX. In all experiments, it was evident that there were two sets of results. Both the LiF, LiOTf, and control experiment with no salt showed low rates of conversion (50–62%) to the organozinc product. In the second set, LiCl, LiBr, and LiI showed full conversion to the organozinc product. These results correlate to our previously mentioned findings with the fluorescence microscopy images, where the oxidative addition intermediate could be more easily solubilized with LiCl, LiBr, and LiI. This observation provides evidence that the rate of conversion observed in macroscale synthesis can be explained by the solubilization effect observed from microscopy experiments.

Furthermore, closer examination of the ^{1}H NMR spectroscopy data reveals prominent differences between the two sets of salts that support structurally different reagents in solution. In the set with LiF, LiOTf, and the no-salt control sample, α methylene protons exhibited at 0.53 ppm, whereas the set with LiCl, LiBr, and LiI exhibited those same protons comparatively upfield at 0.38 ppm. In addition, the protons in the first set revealed first-order coupling patterns. whereas the protons in the second set revealed second-order coupling patterns. These distinct coupling

patterns and chemical environments led to the conclusion that the salts exist as two distinct classes of structural conformity. In the case of LiF or no salt, the organozinc reagent resembles a monomeric structure RZnI, whereas in the case of LiCl, LiBr, and LiI, the organozinc reagent resembles a neutral diorganozinc compound R_2Zn[37,38]. The stark difference in chemical environments and coupling patterns between these two sets provide compelling evidence that the two classes of lithium salts produce reactivity differences on the solubilization of intermediates from the zinc surface.

The difference in solubilization of oxidative addition intermediates and accelerated organozinc formation in macroscale synthesis can be explained by inherent properties of the lithium salt. The anion of the salt must be able to coordinate to zinc to form a zincate, which boasts high solubility. Anions with high propensities for coordination to zinc such as Cl, Br, and I are able to better facilitate the solubilization step and dictate the final solution structure. Salts with low solubility in THF, such as LiF[39], show low propensity of the anion to coordinate to the zinc surface due to strong LiF bonds. The coordinating nature of the cation in solution is also an important factor in the organozinc formation. Enhanced solubility of the organozinc product occurs because of the propensity of the lithium cation to coordinate in THF, resulting in a complex $(THF)_nLi[RZnX_2]$, which results in the release of the organozinc species from the surface, which can then equilibrate into $R_2Zn + Li[ZnX_3]$[40].

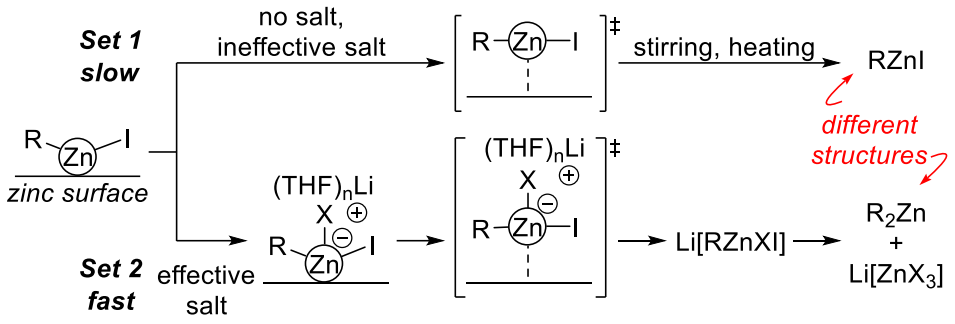

Figure 4. Unifying theoretical and predictive model.

This combined fluorescence microscopy and ^{1}H NMR spectroscopy study shows that the solubilization of the oxidative addition intermediate **2** correlated with the accelerated reaction in the bulk synthesis of the organozinc reagent. The imaging of these intermediates, which were not previously observed due to the insufficient quantities needed for traditional analytical instruments, establish a connection with the observations from macroscale synthesis. The predictive power of this fluorescence microscopy technique could be applied to other systems involving oxidative addition reactions and enable rational development of organometallic reagents.

III. Explaining the High Reactivity of Rieke Zinc

In our previous study[26], we had demonstrated the use of fluorescence microscopy as a tool for preliminary analysis of the macroscale synthesis of organozinc reagents with various lithium salt additives. At this point, single-particle fluorescence microscopy studies have only been used to mechanistically study the formation of organozinc reagent using the method by Knochel[2]. Decades earlier, however, Rieke found another method for organozinc formation which involved the preparation of an activated form of zinc metal[13,14,41]. This activated form of zinc, herein referred to as Zn*, is a highly reactive and a facile tool in organozinc reactions[13–16,42]. Rieke had then developed a toolbox of activated metals including magnesium[19], nickel[43], copper[44], and cobalt[27]. A complete rationale for the high reactivity of these Rieke metals in organometallic

complex formation still remains to be formulated. In the generic preparation of Rieke metals, an alkali metal reduces a metal halide salt, forming the Rieke metal and an alkali metal halide salt. We hypothesize that the presence of a lithium salt byproduct in the formation of Rieke zinc facilitates the high rate of organozinc formation in reactions from Zn* and organohalide substrates. This lithium salt byproduct could plausibly act as a solubilizing agent for the final organozinc product, congruent with the role of the lithium salt[24,25] in the method of organozinc formation by Knochel[2]. We envisioned that using fluorescence microscopy, the presence or absence of oxidative addition intermediates on the surface of the Rieke zinc particles could be visualized in a similar method to our previous study with Jess[26]. The salt byproduct effect on intermediate persistence could then be studied directly.

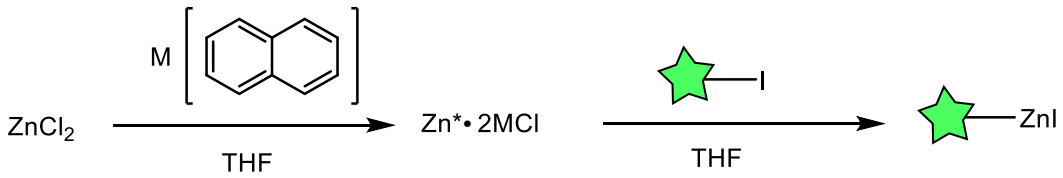

Figure 5. Schematic preparation of Rieke zinc and subsequent reaction with fluorophore-tagged organoiodide substrate. M = Li or Na. Fluorescent tag is the same BODIPY used in study with Jess[26].

In the typical preparation of Zn*[16], lithium metal is first dissolved in a solution of 1.01 equiv of naphthalene in THF, forming a dark green lithium naphthalenide solution. After stirring for 2 h, a solution of 1.75 equiv of $ZnCl_2$ in THF is added dropwise into the lithium naphthalenide while stirring. After the complete addition of $ZnCl_2$, finely divided solid particles will form and the mother liquor should revert back to a colorless solution. Larger Zn* particles can be generated by increasing the speed of the $ZnCl_2$ addition; smaller particles can be generated by further vigorous stirring after the addition. Rieke zinc should resemble fine black particles with varied morphologies. These particles can then either be washed or used immediately for organozinc

synthesis. Since the LiCl byproduct is hypothesized to accelerate organozinc synthesis, this synthesis was configured to generate different salt byproducts in the Zn* particles. For example, sodium naphthalenide was used to generate Rieke zinc with the inclusion of NaCl byproduct.

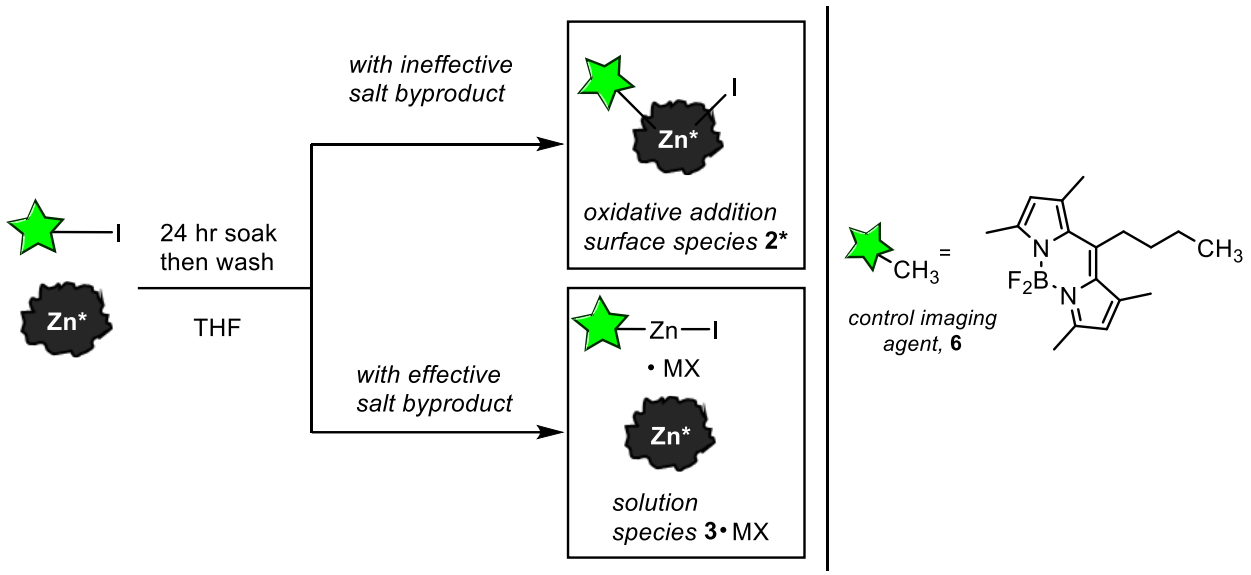

Figure 6. Left: Schematic of the fluorescence microscopy experiments for Rieke zinc, Right: Control imaging agent.

In this study, two forms of Zn* were prepared for analysis by fluorescence microscopy, which were Zn* with the LiCl and NaCl byproduct. These two forms of Zn* will be referred to as Zn*•2LiCl and Zn*•2NaCl, respectively. It should be noted that the Zn*•2NaCl is present mostly as a black suspension in THF which was vigorously washed with THF and yielded only a small amount of very fine black particles. Both these samples were divided in half and were subjected to a 24 h soak in a solution of either **1** or **6** in THF (Figure 6). Imaging agent **6** acts as a control since there is no carbon–iodide bond present, so oxidative addition cannot occur. This method was adapted from the previous method for BODIPY treatment of zinc metal by Feng, and it was found that reducing the concentration of fluorescent marker to 2 µM was ideal for microscopy study of

Zn* particles. After the treatment of Zn* in imaging agent, the supernatant solution was removed and Zn* was thoroughly washed with THF. These Zn* particles were then analyzed by fluorescence microscopy.

One caveat that was discovered during the optimization of microscopy was the choice of solvent under microscopy analysis. Although the reaction and washes were all executed in THF, the Zn* was ultimately transferred into hexanes during the microscopy analysis. When the Zn* particles are left in THF for a prolonged period of time (>5 min), the mother liquor would turn slightly green, indicating fluorescent marker in solution. This was problematic since it caused a high background and poor contrast in the microscopy images. Using a solvent with lower solubility of the imaging agent, such as hexanes, led to less excretion of imaging agent from the Zn* particles, which led to improved image contrast. This hexane imaging protocol was later adopted by other group members for their own projects.

We hypothesized that the reagent Zn*•2LiCl should not have the oxidative addition intermediate **2*** present on the surface and the microscopy images after soak in **1** and **6** would show little or no fluorescence in both cases. In contrast, reagent Zn*•2NaCl should show surface species **2*** since NaCl is an ineffective salt at solubilization, therefore microscopy images of Zn*•2NaCl soaked in **1** should show significant fluorescent hotspots compared to the control soak in **6**.

Fluorescence microcopy analysis of the 4 conditions, however, revealed similar levels of fluorescence between the Zn* soak in **1** and the control **6** for both Zn*•2LiCl and Zn*•2NaCl (Figure 7). Due to the random 3-dimensional nature of the Zn* particles, obtaining a proper focus on the microscope proved difficult. Figure 7 reveals that oxidative addition intermediate is not present in either the type of Zn*, since samples all show the same amount of fluorescence as their

corresponding control. The fluorescent spots present in all of the images are most likely explained by fluorophore trapped within crevices of the Zn* particles. In scanning electron microscopy of Rieke metals, the particles have complicated, sponge-like textures with high surface area[23,45]. Over the 24 h BODIPY soak, imaging agent may have diffused into the microscopic cracks of the Zn* and may not have been accessible to removal during the washing process.

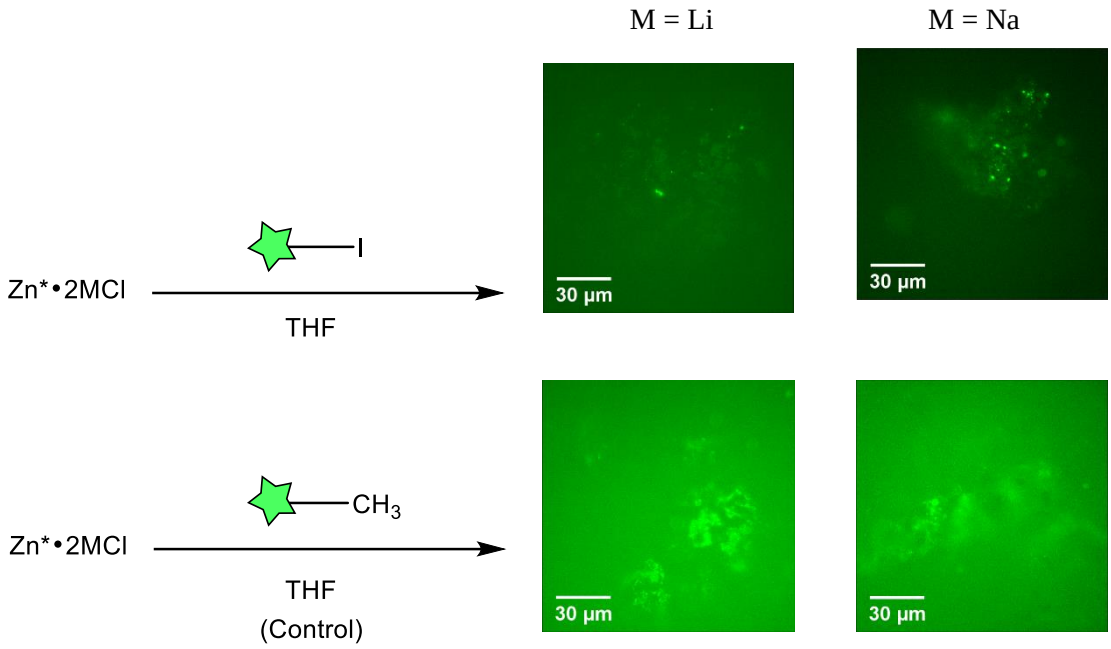

Figure 7. Fluorescence microscopy imaging of Rieke zinc particles after soaking in 2 µM BODIPY solution in THF for 24 h. Laser power in all experiments were kept constant. Brightness settings in ImageJ was set to [75|100] for the M = Li experiments and [100|200] for the M = Na experiments.

To confirm that the fluorescence was not due to oxidative addition intermediate, additional experiments were done where LiCl salt was added to the Zn* particles after soaking in BODIPY solution and subsequent washing (Figure 8). Fluorescence should disappear completely if oxidative addition intermediate is present, but fluorescence should persist after addition of salt if the fluorescence is not due to an intermediate surface species.

Since there is no intermediate present on the Zn* particles in either case, this could be an indication that the solubilization step in oxidative addition occurs so quickly, that the intermediate

cannot be detected. This could be attributed to the high surface area of Zn* which could facilitate release of the organozinc reagent from the surface of the metal. Inherent to the morphology of Zn*, the activation energy for the solubilization step in oxidative addition of substrates could be significantly lower than that of normal zinc metal.

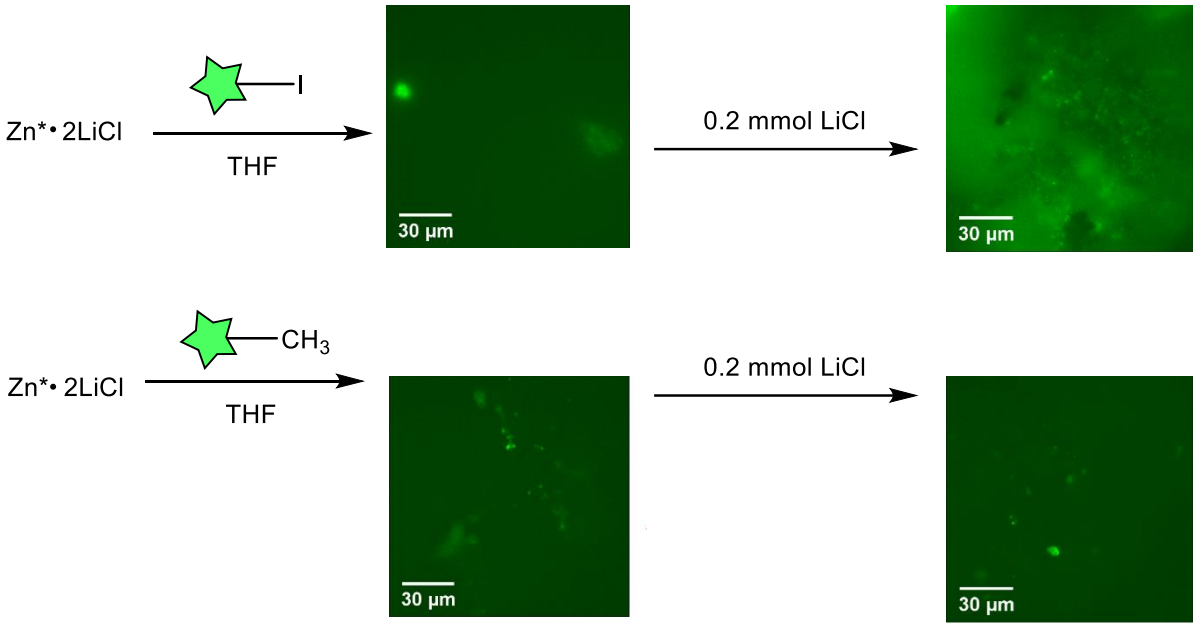

Figure 8. Fluorescence microscopy imaging of Zn • 2LiCl particles after soaking in 2 µM BODIPY solution in THF for 24 h, before and after the addition of LiCl salt. Laser power and brightness was kept constant between all 4 images. Brightness setting in ImageJ was set to [75|200].

The lack of an oxide layer and high surface area on the Rieke metal surface could also explain the high levels of fluorescence found in experiments with Zn* soaked in **1** and control imaging agent **6**. It should not be possible for the control fluorescent marker to perform oxidative addition, however, there is still fluorescence present on these control experiments. Substrate **6** could possibly be attaching to the surface of the Zn* by means of physisorption. On normal zinc metal, physisorption of imaging agent onto the zinc surface is not observed in significant quantities. However, this could be due to the ZnO layer and limited surface area that is present on commercial

zinc powders. Since Zn* does not have an oxide layer present and has more surface area, this could possibly lead to a lower barrier for attachment to the zinc metal, which could explain the fluorescence seen in the control samples.

While this study is still a work in progress, there are certainly other conditions for organozinc formation with Zn* that should be tested. Other lithium halide salts have yet to be tested. Salts such as LiBr and LiI were expected to be effective at solubilizing the organozinc reagent, but since it appears as rapid solubilization is due to the morphology of the Zn* rather than the salt byproduct, then we should expect to see Zn*•2LiBr and Zn*•2LiI to have little difference from Zn*•2LiCl or Zn*•2NaCl. We had attempted to image intermediates in the case of Zn*•2LiF, however the insolubility of ZnF_2 in THF during the Zn* preparation process proved difficult and presented unclear results. It was also unknown if the particles prepared were actually the desired Zn*•2LiF, however this could be characterized by methods such as X-ray photoelectron spectroscopy. Use of other alkali salts besides lithium or sodium have yet to be studied as well. It is possible to prepare Zn* with potassium metal[41], and the preparation of Zn*•2KCl could lead to a more desirable morphology of Zn* particles since naphthalene is not needed. Our lab has also invested in a confocal microscope which will be received after the completion of this thesis, which could provide better resolution of fluorescent hotspots on Zn* due to enhanced imaging ability in 3D.

Overall, fluorescence microscopy has been used to determine that the solubilization step in oxidative addition of organohalide substrates is not accelerated by the alkali salt byproduct present in the Rieke metal. As far as we currently know, this is the first instance of Rieke metals imaged using singe-metal-particle fluorescence microscopy. It was initially believed that the mechanism of organozinc formation was identical to that characterized by Feng,[8] but the absence of oxidative

addition intermediate when Zn* particles prepared with ineffective salts were no different from fluorescence observed from the control fluorophore.

IV. Conclusion

The single-particle fluorescence microscopy technique utilized in both mechanistic studies of organozinc formation proved useful for observing the presence and absence of elementary steps which could not be found in other traditional analytical tools. The high sensitivity of fluorescence microscopy enabled the detection of oxidative addition on the surface of the Zn particles which could not previously be observed due to the lack of significant quantity on the metal surface. These sub-ensemble measurements also revealed the non-uniformity of fluorophore-tagged organic substrates interacting with the zinc surface.

We found that the choice of salt in the synthesis by Knochel[2] plays significant role in the solubilization step of the organozinc reagent and the conversion rate and structure in the macroscale synthesis. The fact that the analysis by fluorescence microscopy and ^{1}H NMR spectroscopy sorted the salts in the same two sets showed how the elementary step of solubilization effected the conversion and structure in the bulk synthesis.

Rieke zinc does not appear to accelerate the rate of organozinc formation in a similar manner to the mechanism found by Feng. Instead of the alkali salt byproduct acting as an agent for solubilization of the ultimate organozinc reagent, it appears as if the solubilization rapidly occurs despite the presence of ineffective salts as a byproduct of the Rieke zinc formation.

Fluorescence microscopy has proved to be a useful tool for observing substances with low levels of detectability. These studies could be further extended to observing intermediates in other systems where oxidative addition occurs on a surface. These studies have aided in pioneering a

novel and highly sensitive analytical technique with excellent spatiotemporal resolution and could prove useful in addition to traditional methods of analysis.

References

(1) Grignard, V. Sur Quelques Nouvelles Combinaisons Organomagnésiennes Mixtes et Leur Application a Des Synthèse d'Acides, d'Alcools et d'Hydrocarbures. *Comptes rendus l'Académie des Sci.* **1900**, *130*, 1322–1325.

(2) Krasovskiy, A.; Malakhov, V.; Gavryushin, A.; Knochel, P. Efficient Synthesis of Functionalized Organozinc Compounds by the Direct Insertion of Zinc into Organic Iodides and Bromides. *Angew. Chemie Int. Ed.* **2006**, *45*, 6040–6044.

(3) Chen, Y.-H.; Knochel, P. Preparation of Aryl and Heteroaryl Indium(III) Reagents by the Direct Insertion of Indium in the Presence of LiCl. *Angew. Chemie Int. Ed.* **2008**, *47*, 7648–7651.

(4) Peng, Z.; Knochel, P. Preparation of Functionalized Organomanganese(II) Reagents by Direct Insertion of Manganese to Aromatic and Benzylic Halides. *Org. Lett.* **2011**, *13*, 3198–3201.

(5) Blümke, T. D. New Preparation of Organoaluminiums – Catalysed Metal Insertion of Aluminium Powder and Synthetic Applications of Organoalanes Preparation of 1 , 2-Bimetallics by Direct Insertion of Aluminium or Zinc Powder. **2012**.

(6) Dagousset, G.; François, C.; León, T.; Blanc, R.; Sansiaume-Dagousset, E.; Knochel, P. Preparation of Functionalized Lithium, Magnesium, Aluminum, Zinc, Manganese, and Indium Organometallics from Functionalized Organic Halides. *Synth.* **2014**, *46*, 3133–3171.

(7) Negishi, E. Palladium- or Nickel-Catalyzed Cross Coupling. A New Selective Method for Carbon-Carbon Bond Formation. *Acc. Chem. Res.* **2002**, *15*, 340–348.

(8) Feng, C.; Cunningham, D. W.; Easter, Q. T.; Blum, S. A. Role of LiCl in Generating

Soluble Organozinc Reagents. *J. Am. Chem. Soc.* **2016**, 11156−11159.

(9) Ochiai, H.; Jang, M.; Hirano, K.; Yorimitsu, H.; Oshima, K. Nickel-Catalyzed Carboxylation of Organozinc Reagents with CO_2. *Org. Lett.* **2008**, *10*, 2681–2683.

(10) Achonduh, G. T.; Hadei, N.; Valente, C.; Avola, S.; O'Brien, C. J.; Organ, M. G. On the Role of Additives in Alkyl-Alkyl Negishi Cross-Couplings. *Chem. Commun.* **2010**, *46*, 4109–4111.

(11) von Frankland, E. Ueber Die Isolirung Der Organischen Radicale. *Justus Liebigs Ann. Chem.* **1849**, *71*, 171–213.

(12) Langer, F.; Schwink, L.; Devasagayaraj, A.; Chavant, P.-Y.; Knochel, P. Preparation of Functionalized Dialkylzincs via a Boron−Zinc Exchange. Reactivity and Catalytic Asymmetric Addition to Aldehydes. *J. Org. Chem.* **1996**, *61*, 8229–8243.

(13) Rieke, R. D.; Uhm, S. J.; Hudnall, P. M. Activated Metals. Preparation of Highly Reactive Zinc. *J. Chem. Soc. Chem. Commun.* **1973**, No. 8, 269b.

(14) Rieke, R. D.; Li, P. T.-J.; Burns, T. P.; Uhm, S. T. Preparation of Highly Reactive Metal Powders. New Procedure for the Preparation of Highly Reactive Zinc and Magnesium Metal Powders. *J. Org. Chem.* **1981**, *46*, 4323–4324.

(15) Rieke, R. D.; Uhm, S. J. An Improved Procedure for the Prepatation of β-Hydroxy Esters Using Activated Zinc. *Synthesis.* **1975**, 452–453.

(16) Zhu, L.; Wehmeyer, R. M.; Rieke, R. D. The Direct Formation of Functionalized Alkyl(Aryl)Zinc Halides by Oxidative Addition of Highly Reactive Zinc with Organic Halides and Their Reactions with Acid Chlorides, α,β-Unsaturated Ketones, and Allylic, Aryl, and Vinyl Halides. *J. Org. Chem.* **1991**, *56*, 1445–1453.

(17) Rieke, R. D. Preparation of Organometallic Compounds from Highly Reactive Metal

Powders. *Science.* **1989**, *246*, 1260–1264.

(18) Rieke, R. D.; Bales, S. E. Activated Metals. The Effect of Added Metal Salts on Magnesium Reactivity. *J. Chem. Soc. Chem. Commun.* **1973**, 879.

(19) Rieke, R. D.; Hudnall, P. M. Activated Metals. I. Preparation of Highly Reactive Magnesium Metal. *J. Am. Chem. Soc.* **1972**, *94*, 7178–7179.

(20) Rieke, R. D.; Kavaliunas, A. V. Preparation of Highly Reactive Metal Powders. Preparation and Reactions of Highly Reactive Palladium and Platinum Metal Slurries. *J. Org. Chem.* **1979**, *44*, 3069–3072.

(21) Takai, K.; Ikawa, Y. Indium-Catalyzed Reduction of Allyl Bromide with Gallium or Aluminum. Formation of Allylgallium and Allylaluminum Sesquibromides. *Org. Lett.* **2002**, *4*, 1727–1729.

(22) Rieke, R. D.; Bales, S. E.; Hudnall, P. M.; Burns, T. P.; Poindexter, G. S. Highly Reactive Magnesium for the Preparation of Grignard Reagents: 1-Norbornanecarboxylic Acid. *Org. Synth.* **1979**, *59*, 85.

(23) Rieke, R. D. *Chemical Synthesis Using Highly Reactive Metals*; John Wiley & Sons, Inc: Hoboken, New Jersey, 2017.

(24) Feng, C.; Cunningham, D. W.; Easter, Q. T.; Blum, S. A. Role of LiCl in Generating Soluble Organozinc Reagents. *J. Am. Chem. Soc.* **2016**, *138*, 11156–11159.

(25) Feng, C.; Easter, Q. T.; Blum, S. A. Structure-Reactivity Studies, Characterization, and Transformation of Intermediates by Lithium Chloride in the Direct Insertion of Alkyl and Aryl Iodides to Metallic Zinc Powder. *Organometallics* **2017**, *36*, 2389–2396.

(26) Jess, K.; Kitagawa, K.; Tagawa, T. K. S.; Blum, S. A. Microscopy Reveals: Impact of Lithium Salts on Elementary Steps Predicts Organozinc Reagent Synthesis and Structure.

J. Am. Chem. Soc. **2019**, *141*, 9879–9884.

(27) Rochfort, G. L.; Rieke, R. D. Preparation, Characterization, and Chemistry of Activated Cobalt. *Inorg. Chem.* **1986**, *25*, 348–355.

(28) Garza-Rodríguez, L. A.; Kharisov, B. I.; Kharissova, O. V. Overview on the Synthesis of Activated Micro- and Nanostructurized Rieke Metals: History and Present State. In *Synthesis and Reactivity in Inorganic, Metal-Organic, and Nano-Metal Chemistry*; 2009; Vol. 39, pp 270–290.

(29) D. Ng, J.; P. Upadhyay, S.; N. Marquard, A.; M. Lupo, K.; A. Hinton, D.; A. Padilla, N.; M. Bates, D.; H. Goldsmith, R. Single-Molecule Investigation of Initiation Dynamics of an Organometallic Catalyst. *J. Am. Chem. Soc.* **2016**, *138*, 3876–3883.

(30) Feng, C.; Easter, Q. T.; Blum, S. A. Structure-Reactivity Studies, Characterization, and Transformation of Intermediates by Lithium Chloride in the Direct Insertion of Alkyl and Aryl Iodides to Metallic Zinc Powder. *Organometallics* **2017**, *36*, 2389–2396.

(31) Roeffaers, M. B. J.; Sels, B. F.; Uji-i, H.; De Schryver, F. C.; Jacobs, P. A.; De Vos, D. E.; Hofkens, J. Spatially Resolved Observation of Crystal-Face-Dependent Catalysis by Single Turnover Counting. *Nature* **2006**, *439*, 572–575.

(32) Esfandiari, N. M.; Wang, Y.; Bass, J. Y.; Cornell, T. P.; Otte, D. A. L.; Cheng, M. H.; Hemminger, J. C.; McIntire, T. M.; Mandelshtam, V. A.; Blum, S. A. Single-Molecule Imaging of Platinum Ligand Exchange Reaction Reveals Reactivity Distribution. *J. Am. Chem. Soc.* **2010**, *132*, 15167–15169.

(33) Cordes, T.; Blum, S. A. Opportunities and Challenges in Single-Molecule and Single-Particle Fluorescence Microscopy for Mechanistic Studies of Chemical Reactions. *Nat. Chem.* **2013**, *5*, 993–999.

(34) Ristanović, Z.; Kubarev, A. V.; Hofkens, J.; Roeffaers, M. B. J.; Weckhuysen, B. M. Single Molecule Nanospectroscopy Visualizes Proton-Transfer Processes within a Zeolite Crystal. *J. Am. Chem. Soc.* **2016**.

(35) Kubarev, A. V.; Janssen, K. P. F.; Roeffaers, M. B. J. Noninvasive Nanoscopy Uncovers the Impact of the Hierarchical Porous Structure on the Catalytic Activity of Single Dealuminated Mordenite Crystals. *ChemCatChem* **2015**, *7*, 3646–3650.

(36) Easter, Q. T.; A. Blum, S. Organic and Organometallic Chemistry at the Single-Molecule, -Particle, and -Molecular-Catalyst-Turnover Level by Fluorescence Microscopy. *Acc. Chem. Res.* **2019**, *52*, 2244-2255.

(37) Stevenson, P. J. Second-Order NMR Spectra at High Field of Common Organic Functional Groups. *Org. Biomol. Chem.* **2011**, *9*, 2078–2084.

(38) Boersma, J.; Noltes, J. G. Properties of Unsolvated Organozinc Halides. *Tetrahedron Lett.* **1966**, *7*, 1521–1525.

(39) Wynn, D. A.; Roth, M. M.; Pollard, B. D. The Solubility of Alkali-Metal Fluorides in Non-Aqueous Solvents with and without Crown Ethers, as Determined by Flame Emission Spectrometry. *Talanta* **1984**.

(40) Hunter, H. N.; Hadei, N.; Blagojevic, V.; Patschinski, P.; Achonduh, G. T.; Avola, S.; Bohme, D. K.; Organ, M. G. Identification of a Higher-Order Organozincate Intermediate Involved in Negishi Cross-Coupling Reactions by Mass Spectrometry and NMR Spectroscopy. *Chem. - A Eur. J.* **2011**, *17*, 7845–7851.

(41) Rieke, R. D.; Uhm, S. J. Activated Metals. XI. An Imporoved Procedure for the Preparation of Beta-Hydroxy Esters Using Activated Zinc. *Synthesis.* **1975**, 452–453.

(42) Rieke, R. D.; Hanson, M. V.; Brown, J. D.; Niu, Q. J. Direct Formation of Secondary and

Tertiary Alkylzinc Bromides and Subsequent Cu(I)-Mediated Couplings. *J. Org. Chem.* **1996**, *61*, 2726–2730.

(43) Rieke, R. D.; Wolf, W. J.; Kujundzic, N.; Kavaliunas, A. V. Highly Reactive Transition Metal Powders. Oxidative Insertion of Nickel, Palladium, and Platinum Metal Powders into Aryl-Halide Bonds. *J. Am. Chem. Soc.* **1977**, *99*, 4159–4160.

(44) Rieke, R. D.; Rhyne, L. D. Preparation of Highly Reactive Metal Powders. Activated Copper and Uranium. The Ullmann Coupling and Preparation of Organometallic Species. *J. Org. Chem.* **1979**, *44*, 3445–3446.

(45) Kudret, S.; Haen, J. D.; Lutsen, L.; Vanderzande, D.; Maes, W. An Efficient and Reliable Procedure for the Preparation of Highly Reactive Rieke Zinc. *Adv. Synth. Catal.* **2013**, *7*, 560–575.

(46) Arnold, R. T.; Kulenovic, S. T. Activated Metals. A Procedure for the Preparation of Activated Magnesium and Zinc. *Synthetic Communications.* **1977**, *7*, 223-232.

(47) Easter, Q. T.; Blum, S. A. Single Turnover at Molecular Polymerization Catalysts Reveals Spatiotemporally Resolved Reactions. *Angew. Chemie–Int. Ed.* **2017**, *56*, 13772–13775.

Appendix 1: General Information

All manipulations were carried out under inert atmosphere using dried glassware unless otherwise noted. Inert atmosphere was nitrogen, unless Li metal was used (mainly for the Rieke zinc experiments), in which case Argon was used. All chemicals were used as received from commercial sources unless otherwise noted. HPLC grade THF, hexanes, and toluene were purchased from Fisher Chemical and dried by passage through an alumina column under argon pressure on a Seca Solvent System (Glass Contour), or by vacuum-transfer from sodium after drying overnight at 100 °C in a sealed Schlenk tube. Zinc powder (Strem, 325 mesh, 99.9%) was dried in vacuo with applying heat from a heat gun until a constant pressure of ca. 50 μbar. Lithium chloride (Sigma-Aldrich), lithium fluoride, lithium bromide (both Alfa Aesar), lithium iodide (Acros), zinc chloride (EMD Millipore Sigma), and zinc fluoride were dried in a Schlenk tube in vacuo with repeated cycles of applying heat from a heat gun and flushing with nitrogen until a constant pressure of ca. 20 μbar at heating was maintained. Trimethylsilyl chloride (Aldrich) was dried by stirring over CaH_2 for 24 h and vacuum transferred. Sodium metal (Alfa Aesar) and lithium rods (Sigma-Aldrich) were stored in glovebox under argon atmosphere. Naphthalene was purchased from Fisher Chemical. THF-d_8 was dried with sodium overnight at 120 °C in a sealed Schlenk bomb tube and vacuum transferred.

1.1 Microscope Parameters

Fluorescence microscopy imaging for the solubilization experiments (section 2.1) was performed with an IX71 inverted microscope (Olympus Corp.) and a 60x oil-immersion objective with a 1.49 numerical aperture. Samples in experiments described in section 2.1 (solubilization experiments) were illuminated with the 488 nm line of an Ar/Kr ion laser (Coherent Inc.) with power above the objective ca. 0.3–0.4 mW. Illumination of sample was conducted under

conditions of widefield EPI fluorescence. Samples were imaged with a C9100-13 electron multiplier CCD camera (Hamamatsu Photonics). The CCD chip was a black-thinned electron multiplication type with an effective 512 × 512 array of pixels and pixel width and height of 0.267 μm.

Fluorescence microscopy equipment was upgraded before the Rieke zinc experiments started (section 4.1–4.2). Samples were, again, using the same Olympus microscope and an oil-immersion, 60x objective with a 1.49 numerical aperture. Samples on fluorescence microscope were illuminated with the 488 nm line obtained from a solid-state laser stack (Intelligent Imaging Innovations). Samples were imaged with a CMOS Prime 95B camera (Photometrics). The Backside Illuminated Sensor (95% quantum efficiency) has an effective 1200 × 1200 array of pixels. The pixel size was 11 μm, which with the 60x magnification, resulted in each pixel in the acquired images representing an area of 115 × 115 nm. Time lapses were obtained at gain = 1, 100 ms exposure, with intervals every 1000 ms.

The focus of the microscope was changed with a z-axis controller (MS-2000, Applied Scientific Instruments, Inc.).

Reaction cells were constructed from a 4 mL screw-cap vial by cutting the bottom of the vials and adhering them to a prepared glass cover slip with Devcon Epoxy as previously reported.[1] The epoxy was allowed to cure overnight and then brought into the glovebox. Glass pockets were made from Pasteur pipettes as previously reported.[8]

Appendix 2: Solubilization Experiments (Fluorescence Microscopy)

All of the following manipulations were done in a nitrogen-filled glovebox. To prepare the 2.0 mM BODIPY stock solution, BODIPY **2** (1.7 mg, 4.0 μmol) was dissolved in THF (2.0 mL).

2.1 Salt Addition Experiments

Figure S1 schematically shows the procedure to obtain the microscopy images. A widefield microscopy approach was selected because it acquires the full field of view image at the same time. This approach is well-suited to viewing the behavior of multiple zinc particles at the same time. (In contrast, confocal microscopy involves scanning the sample during image acquisition, results in different parts of the image being acquired at different times.) Zinc (75 mg, 1.2 mmol) was weighed in a 4 mL screw-cap vial and treated with THF (1 mL) and TMSCl (1 drop), consecutively, and then the vial was capped and agitated. After 2 h soaking at room temperature the solution was removed by syringe and the powder washed with THF (3 × 1 mL). After the last wash and removal of the washing solution, the powder was treated with the 2.0 mM stock solution of 1 (10 drops), the vial was capped and agitated (A, Figure S1). This mixture was allowed to soak at room temperature for 20 h. After that time, the solution was removed by syringe and the powder washed three times with THF (3 × 1 mL). After the last wash and removal of the washing solution, additional clean THF (3 mL) was added (B).

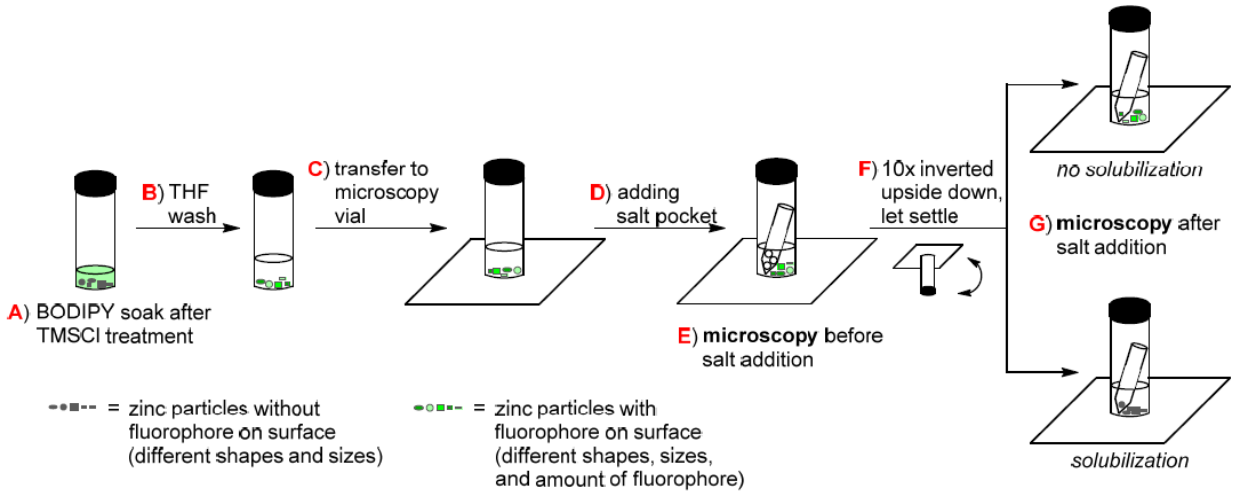

Figure S1. Schematic procedure to obtain microscopy images. The same supplier and mesh of zinc particles were used as in the reported synthetic procedure by Knochel, allowing detection of the heterogeneity of reactivity germane to the "real" synthetic reaction. This heterogeneity involved a range of particle sizes, shapes, and chemical compositions. These particles reacted differently, and even different locations on the same particle were found to vary significantly in their reactivity, as detected as a range of brightness and distribution of fluorescent intermediate **2**. This distribution is uniquely revealed by the sensitivity and spatial resolution of the microscopy approach. This heterogeneity is depicted schematically in this figure as different sizes, shapes, and brightness of the particles.

After the first time-lapse prior to salt addition was taken, the microscopy vial was inverted ten times to distribute the salt into the imaging volume and then agitated (**F**). This action rearranges all particles making it impossible to find the exact same particles before and after salt addition. Thus, a new region of the sample was examined. Nevertheless, clear trends are visible across entire samples, which are fully reproducible in triplicate experiments. The next time-lapse was started at t = 90 s after salt addition, which was just after the time it took to place the vial on the microscope and refocus the sample (**G**). For the time-lapse, the same parameters as described above were used.

Using ImageJ to set display conditions for all images, all images in this series are displayed with the same brightness and contrast settings to allow for direct comparison. From the center of the time lapse, an area of 300 × 300 pixels was cropped for display. One frame was chosen that was the best representation of data from the whole video. All experiments were run in triplicate.

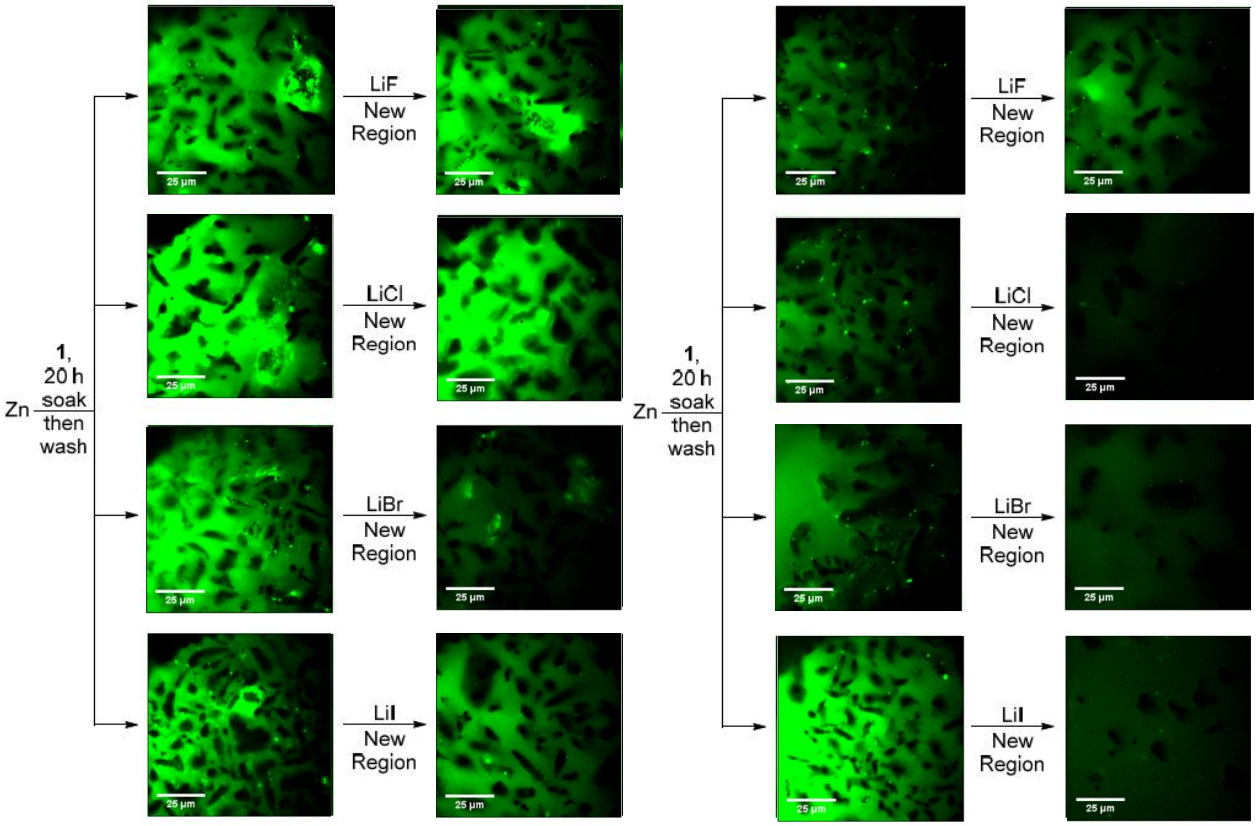
Zn
1, 20 h soak then wash
LiF
New Region
LiCl
New Region
LiBr
New Region
LiI
New Region
25 µm

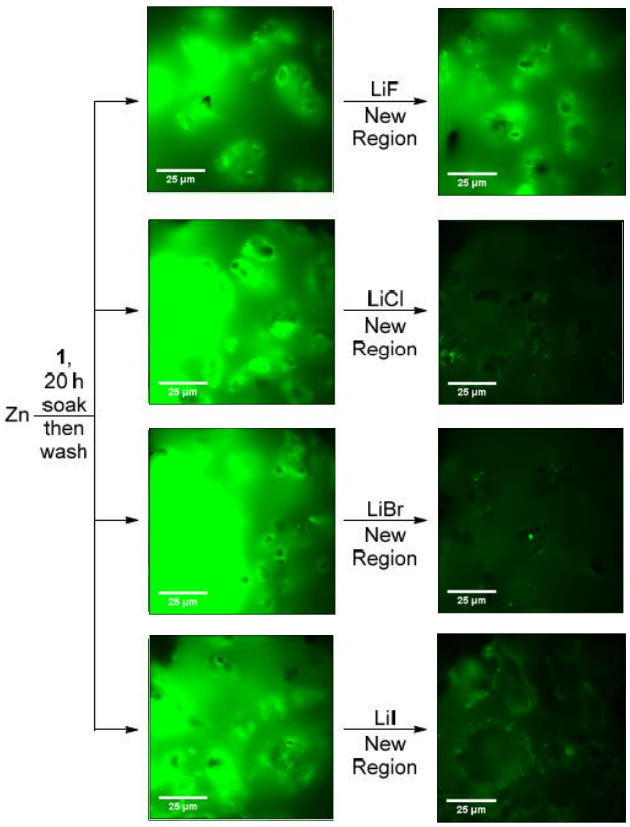

Figure S2. Results from the first, second, and third runs of the salt addition experiments. All images are displayed at identical brightness/contrast settings showing the variation in brightness between samples. Although absolute brightness was different between samples, reflecting the heterogeneity of the samples, the same trend for each salt before and after addition is observed in all triplicate runs. The pictures on the right were taken 90 − 150 s after salt addition. The image after LiI should be regarded with care due to significant fluorescence quenching of iodide.

Appendix 3: NMR Experiments

3.1 Purification of (2-Iodoethyl)benzene

To remove iodine, (2-iodoethyl)benzene (Sigma-Aldrich, 97%) was dissolved in ethyl acetate, and shaken with a saturated aqueous $Na_2S_2O_3$ solution. The aqueous layer was extracted (3 × ethyl acetate) before the combined organic extracts were dried over Na_2SO_4 and the solvent was then evaporated by rotovap. Under nitrogen atmosphere (2-iodoethyl)benzene was added to Schlenk flask that was charged with a stir bar and CaH_2 and stirred overnight to remove water that was not removed during the Na_2SO_4 step. During the first 2 h the flask was kept under dynamic nitrogen to allow for escape of H_2, and afterward it was kept under static nitrogen. After this process, it was fractionally distilled.

3.2 Preparation of the 0.1 M Stock Solution of (2-Iodoethyl)benzene

A stock solution in THF-d_8 with the substrate (2-iodoethyl)benzene (0.1 M) and mesitylene as internal standard (0.1 M) was prepared. The following shows an example procedure to prepare 3.5 mL of this stock solution: All of the following manipulations were done in a nitrogen-filled glovebox. Mesitylene (42.1 mg, 0.350 mmol) and (2-iodoethyl)benzene (81.2 mg, 0.350 mmol) were weighed in separate vials; (2-iodoethy)benzene was weighed in the glass vial with the help of a Pasteur pipette. To the mesitylene vial, 1.0 mL THF-d_8 was added and after that the solution was transferred by Pasteur pipette to the vial of (2-iodoethyl)benzene. This rinsing procedure was repeated once again with 1.0 mL and once with 1.5 mL THF-d_8 (total amount of THF-d_8: 3.5 mL). The vial of the resulting stock solution was tightly capped.

3.3 ^{1}H NMR Experiments

In a nitrogen-filled glovebox, one 4 mL screw-cap vial was charged with zinc (4.6 mg, 0.070 mmol) and a stir bar. Another vial was charged with the corresponding LiX salt [1.3 mg (LiF), 2.1

mg (LiCl), 4.3 mg (LiBr), 6.7 mg (LiI), 7.8 (LiOTf); 0.050 mmol]. My role in this study was to perform experiments with LiF, LiCl, LiBr and LiI for 2 hours at 1500 rpm. First, the 0.1 M stock solution (0.50 mL, i.e., 0.050 mmol substrate and mesitylene) was added to the vial with the lithium salt and agitated until dissolution (LiF gave a fine suspension only; LiCl needed to be shaken vigorously for about 3 min for complete dissolution; LiBr, LiI and LiOTf dissolved rapidly). This mixture was then added to the zinc vial, which was then tightly capped and placed in a metal block on top of a magnetic stirrer to stir without heating at a starting ambient temperature (26–29 °C) for 1 or 2 h, with stirrer speed of 200 rpm or, in case of stirrer speed of 1500 rpm, the batch of vials was placed in an otherwise empty small beaker (but including a tissue wipe for stability, Figure S4). The beaker was fixed ca. 3 cm above the stir plate to exclude unintentional warming of the sample due to the motor in the magnetic stirrer. After the noted reaction time the stirring was stopped. To remove residual zinc metal powder, the mixture was filtered through a filter pipette, a pipette stuffed with a small plug of Whatman GF/B glass microfiber filter, and the filtrate was expelled directly into an NMR tube. The NMR tube was sealed and removed from the glovebox, and spectra were acquired on a Bruker DRX500 spectrometer.

3.4 Integration Values

The following Table S2 shows the integration values and the calculated conversion from the NMR spectra shown in Figure S6 to Figure S11. Conversion was calculated from the integration values of substrate and the corresponding stock solution for that experiment: [1–(Integration$_{\text{Substrate}}$/Integration$_{\text{Stock Solution}}$)]. In cases marked ">99%", the amount of remaining starting material was so low as to not give meaningful integration by spectroscopy, leading to the "negative" integration values noted, even after baseline correction.

Table S1: Values of NMR integration and calculated conversion. My only role in this study was for entries 1-5.

Entry	Experiment	Integration value[a]	Conversion [%]:[b]
	Stock Solution (A)	1.9276	-
1	Zn only, 1500 rpm, 2 hours	0.8254	57
2	LiF, 1500 rpm, 2 hours	0.8496	56
3	LiCl, 1500 rpm, 2 hours	0.0119	99
4	LiBr, 1500 rpm, 2 hours	0.0154	99
5	LiI, 1500 rpm, 2 hours	-0.0076	>99
6	LiOTf, 1500 rpm, 2 hours	0.7322	62

[a] Methylene protons on iodine (α protons) were integrated (integrated region: 3.416-3.309 ppm) and referenced to the mesitylene-CH_3 signal (integrated region: 2.391-2.050 ppm), which was set to 9 protons. [b] Calculated from the integration values of substrate and the corresponding stock solution for that experiment: [1–(Integration$_{Substrate}$/Integration$_{Stock\ Solution}$)].

3.5 ^{1}H NMR Spectra (Stock Solution Experiments)

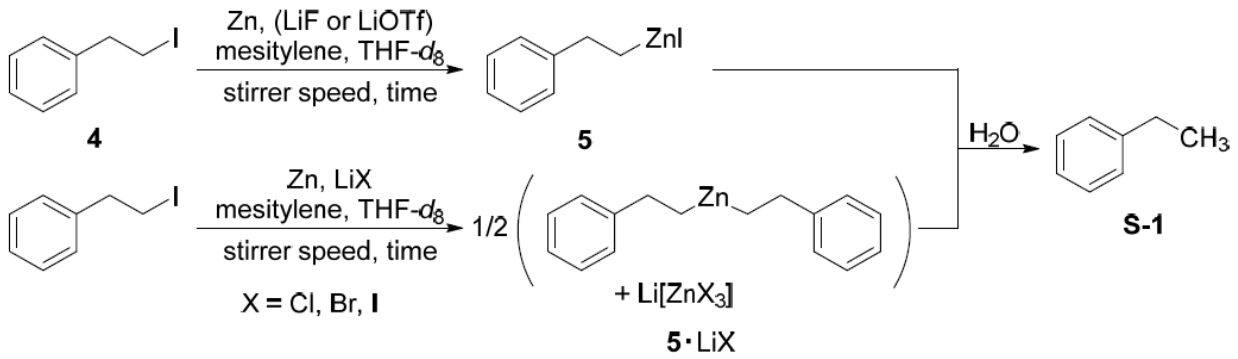

All spectra were referenced to the high field residual proton signal of THF-d_8: δ = 1.72 ppm, at 500 MHz. Signals observed (br: broad, s: singlet, t: triplet, q: quartet, m: multiplet, at: apparent triplet):

2-(Iodoethyl)benzene (**4**): 7.28–7.22 (m, 2H, aromatic), 7.22–7.16 (m, 3H, aromatic), 3.40–3.34 [m (AA'XX'), 2H, CH_2–I], 3.16-3.11 (at, 2H, CH_2–Ph) ppm.

5: 7.25–7.21 (m, 2H, aromatic), 7.17–7.13 (m, 2H, aromatic), 7.03–6.99 (m, 1H, aromatic), 2.81 (at, 2H, CH_2–Ph), 0.53 (at, 2H, CH_2–Zn) ppm.

5·LiCl: 7.21-7.16 (m, 2H, aromatic), 7.12–7.08 (m, 2H, aromatic), 6.98–6.93 (m, 2H, aromatic), 2.80–2.74 [m (AA'XX'), 2H, CH_2–Ph], 0.40–0.36 [m (AA'XX'), 2H, CH_2–Zn] ppm.

5·LiBr: 7.21–7.16 (m, 2 H, aromatic), 7.12–7.08 (m, 2H, aromatic), 6.97–6.93 (m, 2H, aromatic), 2.79-2.73 [m (AA'XX'), 2H, CH_2–Ph], 0.41–0.36 [m (AA'XX'), 2H, CH_2–Zn] ppm.

5·LiI: 7.21–7.16 (m, 2 H, aromatic), 7.12–7.06 (m, 2H, aromatic), 6.97-6.92 (m, 2H, aromatic), 2.78–2.73 [m (AA'XX'), 2H, CH_2–Ph], 0.42–0.36 [m (AA'XX'), 2H, CH_2–Zn] ppm.

Ethylbenzene (**S-1**): 2.61 (q, $^3J_{H,H}$ = 7.7 Hz, 2H, CH_2), 1.20 (t, $^3J_{H,H}$ = 7.6 Hz, 3H, CH_3) ppm. Aromatic signals not identified.

Mesitylene: 6.75-6.73 (m, 3H, C*H*), 2.22-2.21 (m, 9H, CH_3) ppm.

THF-d_7: 3.58 (br. m), 1.72 (br. m) ppm.

water: 2.46 (s) ppm.

silicone grease: 0.11 (s) ppm.

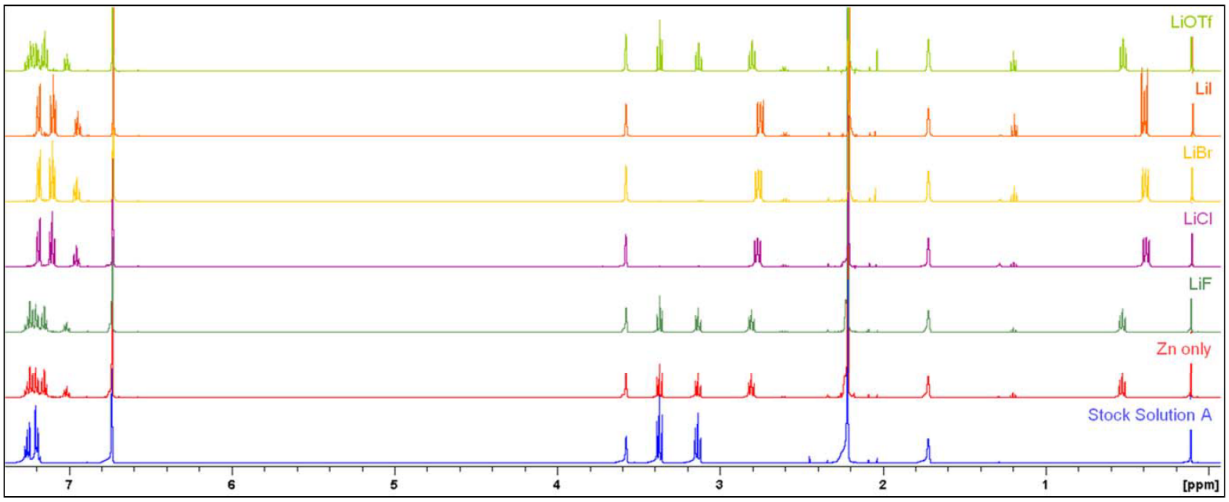

Figure S3: Full ^{1}H NMR spectrum (500 MHz, THF-d_8, 300 K) of experiments with Stock Solution A. Reaction conditions: 1500 rpm, 2 hours. My role in this figure was performing the experiments for all conditions, except for LiOTf.

Appendix 4: Rieke Zinc Microscopy Experiments

All of the following manipulations were done in an argon-filled glovebox. To prepare the 2.0 µM BODIPY stock solution, 0.1 mL of the 2 mM BODIPY **1** solution (previously made in section 2) was diluted with 0.9 mL of THF to yield a dilution of 0.2 mM. This dilution was then diluted again by a factor of 100 (0.02 mL of 0.2 mM solution diluted with 2 mL THF).

4.1 Preparing Rieke Zinc

4.1.1 Zn•2LiCl*

Rieke zinc with LiCl byproduct was synthesized by reducing $ZnCl_2$ with Li naphthalenide.[16,46]

First the Li naphthalenide was generated under argon atmosphere. The Li (20.6 mg, 2.88 mmol) was cut from a lithium rod with metal spatula, with oxide layer cut from metal beforehand, and charged into a 20 dram borosilicate glass scintillation vial along with a Pyrex® encapsulated stir bar. (Pyrex® is preferred because lithium metal can react with Teflon® coated stir bars.) In a 1 dram scintillation vial, naphthalene (373.0 mg, 2.910 mmol) was dissolved with 1.0 mL THF. The resulting naphthalene solution was transferred into the 20 dram vial of Li with a Pasteur pipette. The 20 dram vial and pipette were rinsed with 0.5 mL THF and the rinse was delivered into a 20 dram vial. The 20 dram vial was then sealed with an open-top polypropylene cap lined with PTFE/silicone. The 20 dram vial was then placed on stir plate and was stirring speed was *gradually* increased to 500 rpm and the resulting dark green solution was allowed to stir for exactly 2 h. Careful: Rapid increase in stirring speed or prolonged stirring can result in glass on the stir bar or the vial weakening and possibly shattering! A separate 1 dram scintillation vial was charged with anhydrous $ZnCl_2$ (259.2 mg, 1.902 mmol), which was then fully dissolved in THF (1.5 mL) with the aid of a Pasteur pipette. After the Li naphthalenide solution had stirred for 2 h, the $ZnCl_2$ solution was then loaded into a 3 mL Norm-Ject™ plastic syringe and then *slowly* added dropwise

into the 20 dram vial *while continually stirring* over 5 min. The solution in the 20 dram vial turned colorless, with finely divided black particles of Zn*•2LiCl after complete addition of $ZnCl_2$. The particles were left to stir for 30 min more in order to obtain finer particles for optimal microscopy imaging. The stirring was then stopped and the supernatant THF solution was then removed with a Pasteur pipette and the Zn* particles were then washed with 3 × 3 mL aliquots of THF solution (suspension of Zn* was allowed to quickly settle between washes) before being left stored in a vial under clean THF (3 mL) for up to 1 week.

4.1.2 Zn•2NaCl*

Rieke zinc with NaCl byproduct was prepared in an identical fashion to the previous Zn*•2LiCl procedure.[3] However, this was a *very* low-yielding method of producing Zn*•2NaCl particles suitable for microscopy.

Under nitrogen or argon atmosphere, Na (71.8 mg, 3.12 mmol) was cut from a chunk of sodium metal with a metal spatula, with the oxide layer cut from the metal beforehand, and charged into a 20 dram scintillation vial, along with a Teflon®-coated stir bar. In a 1 dram vial, naphthalene (405.4 mg, 3.163 mmol) was dissolved with 2.5 mL THF. The resulting naphthalene solution was then transferred into the 20 dram vial of Na with a pipette. The 1 dram vial and pipette were rinsed with 0.5 mL THF and the rinse was delivered into the 20 dram vial. The 20 dram vial was then sealed with an open-top polypropylene cap lined with PTFE/silicone. The 20 dram vial was then placed onto a stir plate and the stirring speed was *gradually* increased to 500 rpm. The resulting dark green solution was allowed to stir for 2 h. Another clean 1 dram glass vial was charged with anhydrous $ZnCl_2$ (245.9 mg, 1.804 mmol) and fully dissolved in THF (2.0 mL). The $ZnCl_2$ solution was then loaded into a 6 mL Norm-Ject™ plastic syringe and then *quickly* added into the 20 dram vial of Na naphthalenide *while continually stirring*. The resulting Zn*•2NaCl will form mostly as

a black suspension with *some* finely divided particles. The whole $ZnCl_2$ solution was added all at once in order to obtain some sizable particles at the bottom of the vial. The particles were then left to stir for 30 min more in order to obtain appropriately sized particles for imaging. The stirring was stopped and most of the supernatant solution with Zn* suspension was then removed with a Pasteur pipette. The fine Zn* particles were washed with 3 mL aliquots of THF until supernatant solution remained mostly colorless (the amount of washes with THF varied for each preparation, roughly 7–10 washes. Careful: Zn* particles can be very difficult to see. A small amount of Zn*•2NaCl (roughly 5–10 mg) remained and was stored under clean THF (3 mL) for up to 1 week.

4.1.3 Zn•2LiF*

Zn* with LiF byproduct was synthesized by reducing ZnF_2 with Li naphthalenide. Synthesis of Zn*•2LiF was adapted from LiCl counterpart, however, adjustments were made to account for low solubility of ZnF_2 in THF. As far as we know, this is currently the first reported synthesis of Rieke zinc with LiF as a salt byproduct.

First, Li naphthalenide was generated under an argon atmosphere. The Li (19.3 mg, 2.78 mmol) was cut from a lithium rod with a metal spatula, with the oxide layer cut from the metal beforehand, and charged into a 20 dram borosilicate scintillation vial along with a Pyrex® encapsulated stir bar. In a 1 dram scintillation vial, naphthalene (360.7 mg, 2.814 mmol) was dissolved with 1.0 mL THF. The resulting naphthalene solution was transferred into 20 dram vial with a Pasteur pipette. The 1 dram vial and pipette were rinsed with 0.5 mL THF and the rinse was delivered into 20 dram vial. The 20 dram vial was then sealed with a polypropylene cap. The 20 dram vial was then placed onto a stir plate and stirring speed was *gradually* increased to 500 rpm. The resulting dark green solution was allowed to stir for exactly 2 h. Careful: Rapid increase in stirring speed or prolonged stirring can result in glass on the stir bar or the vial weakening and

possibly shattering! A separate 20 dram glass vial was charged with anhydrous ZnF_2 (165.0 mg, 1.596 mmol) and THF (1.5 mL). Note: ZnF_2 does NOT dissolve in THF. After the Li naphthalenide solution had stirred for 2 h, the resulting solution was transferred by Pasteur pipette into the 20 dram vial of mostly undissolved ZnF_2 in THF. The stir bar was also transferred. The solution was then allowed to stir at 500 rpm for 1 h. The resulting Zn* appeared mostly as a suspension with some fine particles, similar to the appearance of Zn*•2NaCl after addition of $ZnCl_2$ salt. The stirring was stopped and most of the supernatant solution with Zn* suspension was removed with a Pasteur pipette. The remaining Zn* particles were washed with 5 × 3 mL aliquots of THF until the supernatant solution remained colorless. A small amount of Zn•2LiF (roughly 5–10 mg) remained and was stored under clean THF (3 mL) for up to 1 week.

4.2 BODIPY soak of Zn•2MX Particles*

Previously prepared Zn* particles (with any salt byproduct) with its supernatant THF solvent was transferred by Pasteur pipette into a 1 dram scintillation vial; Only about 1–5 mg was needed, enough to cover approximately 1/8 of the bottom of the vial. The suspension settled quickly (<30 s) and the supernatant THF was then removed with a pipette. A dilute solution of fluorescent imaging agent **1** in THF was pipetted directly onto the Zn* particles (10 drops, 2 μM). The Zn* particles were then allowed to soak in fluorescent solution for 20-24 h. Once the soak was complete, the supernatant solution was removed with a pipette and Zn* was washed with THF (3 × 1 mL). After washes, the vial of Zn* remained uncapped in the argon–filled box, which was allowed for drying of any residual THF (5 min). Dry hexane (1 mL) was pipetted into the Zn* vial. A pipette was then used to suspend the Zn* particles in the hexanes and to transfer the suspension into a prepared microscopy vial.

Rieke zinc samples were separately subjected to soaking in fluorescent imaging agent **6** for a control study. The same method mentioned in the previous paragraph was used for these control experiments, with the exception that a solution of **6** in THF (10 drops, 2 μM) was used in place of **1**. The control sample was run at the same time with the same batch of Zn* for the same amount of time as the sample soaked in **1**.

Microscopy vials containing both the Rieke Zn* samples after soak in **1** and **6** were capped, removed from glovebox, and placed on the microscope.

Using ImageJ to set display conditions for all images, all images of the same batch of Zn* are displayed with the same brightness and contrast settings (specific settings shown in Figure S4) to allow for direct comparison. One frame was chosen that was the best representation of data from the whole video. The experiments with Zn*•2LiCl and Zn*•2NaCl were run in triplicate and

duplicate respectively (in addition to first run shown in the manuscript, Figure 7, see Figure S4 for duplicate and triplicate data). One experiment was performed with Zn*•2LiF, but no fluorescent hotspots were visible on Zn* particles and it was difficult at the time of the experiment to determine if the desired Zn* product and salt byproduct had formed.

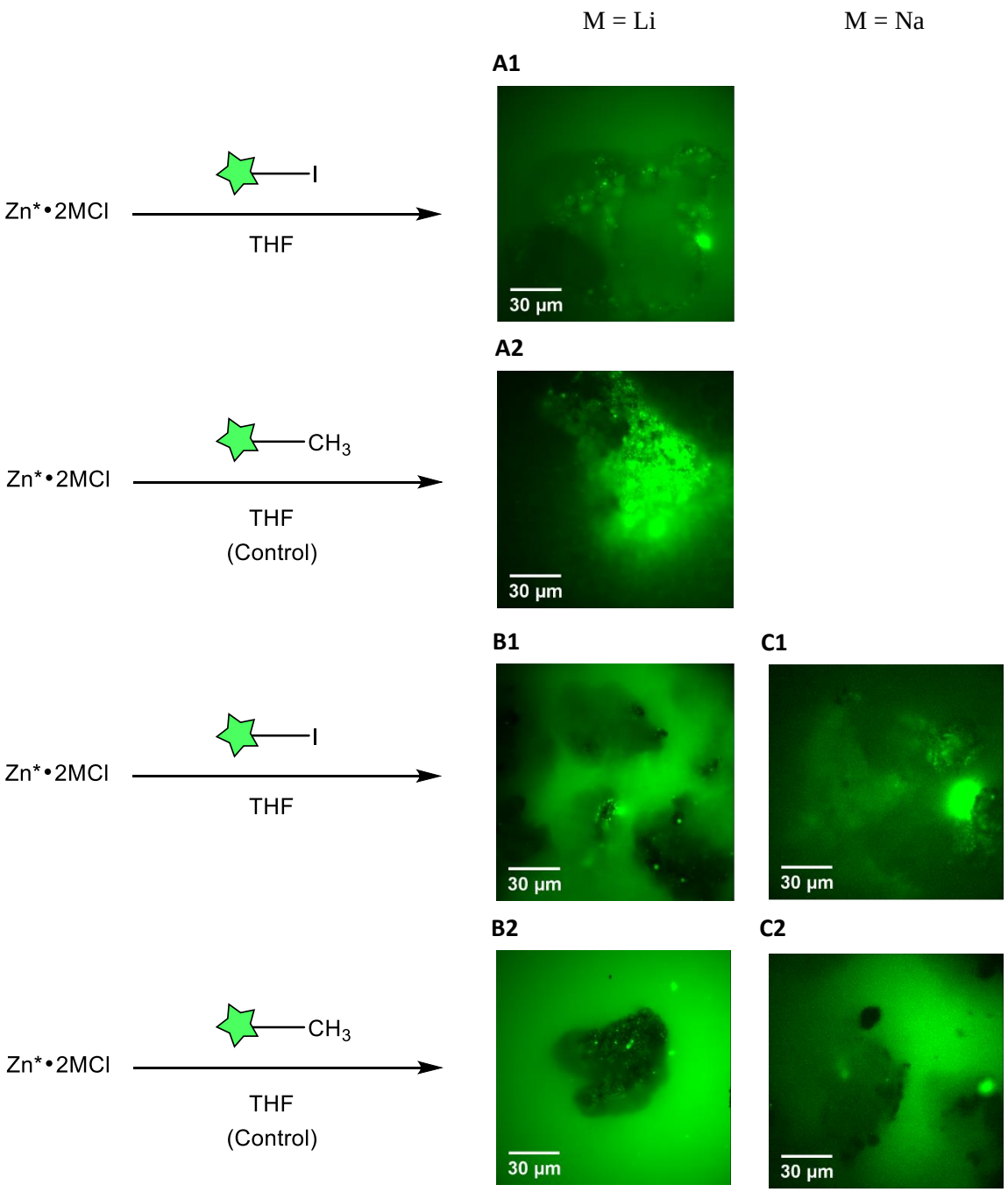

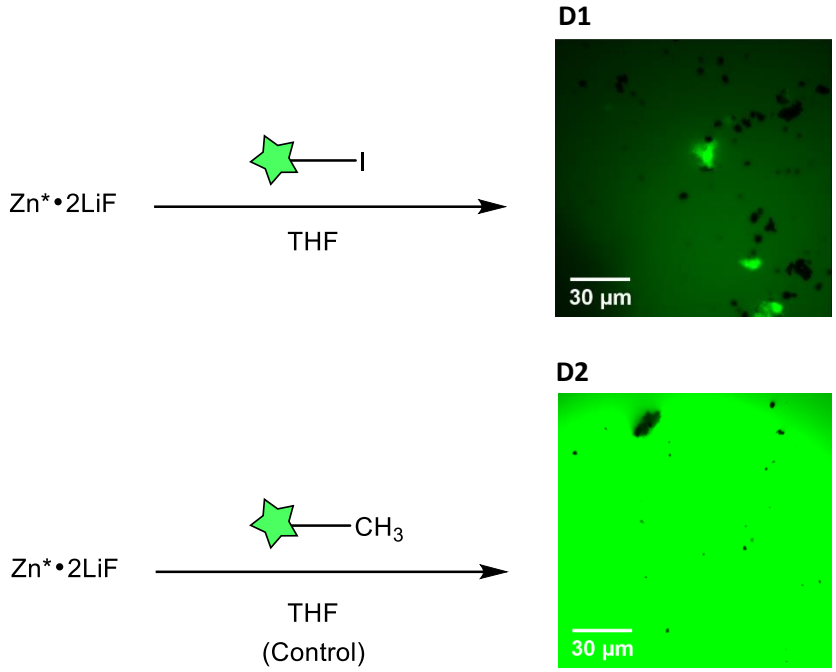

Figure S4. Results from the duplicate and triplicate experiments with Zn*•2LiCl and a duplicate experiment for Zn*•2NaCl. Images are displayed at identical brightness/contrast settings between corresponding samples and controls. Triplicate run for Zn*•2NaCl and Zn*•2LiF is still needed as both are difficult to prepare. The following table provides the various imaging setting for the above experiments.

Image	Laser Power (% of ~6.0 mW)	Exposure (ms)	ImageJ Min Displayed Value	ImageJ Max Displayed Value
A1	1	100	100	2500
A2	1	100	100	2500
B1	1	100	100	2500
B2	1	100	100	2500
C1	1	100	100	150
C2	1	100	100	150
D1	1	100	100	4000
D2	1	10	100	4000

4.3 Zn and LiCl Salt Addition Experiments*

Glass pockets were made from Pasteur pipettes as previously reported.[8] Another sample of Zn*•2LiCl was prepared and soaked in imaging agents **1** and **6**, following the procedure previously mentioned in 4.1 However, a glass pocket charged with LiCl salt (8.6 mg, 2.0 mmol) was placed into each microscopy vial before the vial was capped, removed from the glovebox, and placed on the microscope. Initial captures reveal some fluorescence on the Zn* particles in both the sample and control experiments. After the initial captures, microscopy vials were then inverted 10 times

to mix LiCl with Zn*, identical to the procedure shown in Figure S1. The particles were then imaged on the microscope again, and they showed a similar amount of fluorescence. This result was interpreted to indicate an absence of oxidative addition intermediate since the material did not solubilize. Duplicate and triplicate runs of LiCl salt addition are still needed.

Appendix 5: Synthetic Methods

5.1 Imaging Agents

*5.1.1 Imaging Agent **1** Precursor*

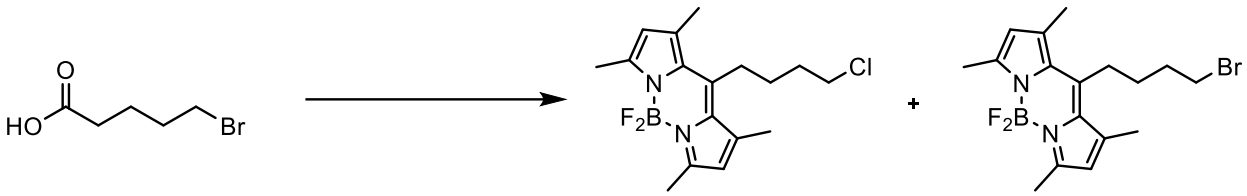

S1

An oven-dried 100-mL round-bottom flask was charged with 5-bromovaleric acid (1268.8 mg, 7.0088 mmol, Acros) and a stir bar, and then placed under dynamic nitrogen atmosphere. Dry CH_2Cl_2 (25 mL) and dry dimethylformamide (0.02 mL, 0.03 mmol, Omnisolve) were added to dissolve the solid and the solution was stirred. Oxalyl chloride (0.66 mL, 7.7 mmol) was added dropwise over 1 min via syringe causing a slow evolution of gas. After the evolution of gas subsided, the solution was stirred at room temperature for 1 h. The solution was then concentrated in vacuo via rotary evaporation to yield a pale-yellow oil, then further concentrated on a high vacuum line for 1 h to remove excess oxalyl chloride (WARNING: HCl will be evaporated off. It is advised to close off line to any pressure gauges to prevent damage). The acid chloride was dissolved in dry CH_2Cl_2 (25 mL) and the solution was stirred. Phosphorus oxychloride (0.71 mL, 7.6 mmol) was added via syringe, followed by the addition of 2,4-dimethylpyrrole (1.80 mL, 17.4 mmol, TCI) dropwise via syringe over 1 min. The mixture was stirred at reflux for 5 h under static nitrogen atmosphere (round-bottom flask was sealed with a septum tightened with copper wire). The solution was then cooled to room temperature, and concentrated via rotary evaporation to yield a viscous, dark orange-red mixture. Mixture was layered with hexanes (80 mL) and the mixture was stored at –35 °C overnight.

The hexanes were decanted and the residue was placed under high vacuum for 1 h. The residue was then dissolved in dry toluene (30 mL) and treated with triethylamine (1.4 mL, 11 mmol, Fisher Scientific). The solution was stirred for 1 h at 80 °C. Boron trifluoride dimethyl etherate (0.86 mL, 9.4 mmol, Sigma-Aldrich) was added via syringe, and the mixture was stirred at 80 °C for 1 h. The red solution was cooled to room temperature and then washed with water (3 × 50 mL) and brine (3 × 50 mL). The organic layer was dried over sodium sulfate, filtered, and concentrated in vacuo to yield a dark red solid. The solid was purified by flash chromatography (CH_2Cl_2:hexanes (1:1), Rf = 0.35) to yield a bright orange solid (literature yield: 15%[47], 10:1 mixture of chloride to bromide). Solid **S1** was then repurified using the same method, yielding 389.8 mg (16.4% yield), 90.8:9.2 BODIPY-Cl/Br.

*5.1.2 Imaging Agent **1***

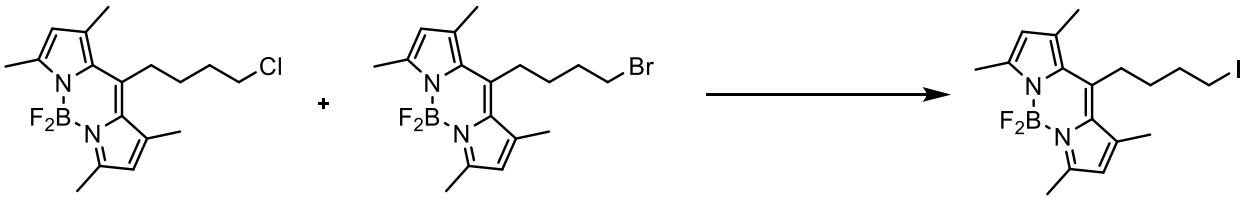

S1 **1**

Fluorescent probe **1** was synthesized via a Finkelstein reaction. A 1 dram scintillation vial was charged with sodium iodide (170.2 mg, 1.135 mmol), acetone (3.0 mL), followed by precursor S1 (110.5 mg, 0.3268 mmol). After heating at reflux for 8 h, the reaction mixture was evaporated to dryness. The residue that remained was dissolved in CH_2Cl_2 (ca. 10 mL), extracted with brine then water (ca. 5 mL each), and dried over sodium sulfate. The mixture was filtered to removed sodium sulfate and then concentrated in vacuo to yield a crude product which was then chromatographed with 25% DCM in hexanes as the eluent. Removal of volatiles at ca. 10 mTorr for 6 h afforded **1** as an orange solid (51.6 mg, 37% yield). ^{1}H NMR ($CDCl_3$, 600 MHz) δ 6.06 (s,

2H), 3.22 (t, *J* = 6.8 Hz, 2H), 2.98 (t, *J* = 8.5 Hz, 2H), 2.51 (s, 6H), 2.43 (s, 6H), 2.03 (quin, *J* = 7.2 Hz, 3H). HRMS (ESI): m/z calculated for $C_{17}H_{22}BF_2IN_2Na$ ($[M+Na]^+$), 453.0790; found, 453.0366.

*5.1.3 Imaging Agent **6***

Control probe **6** was previously synthesized in our lab as previously reported.[32]

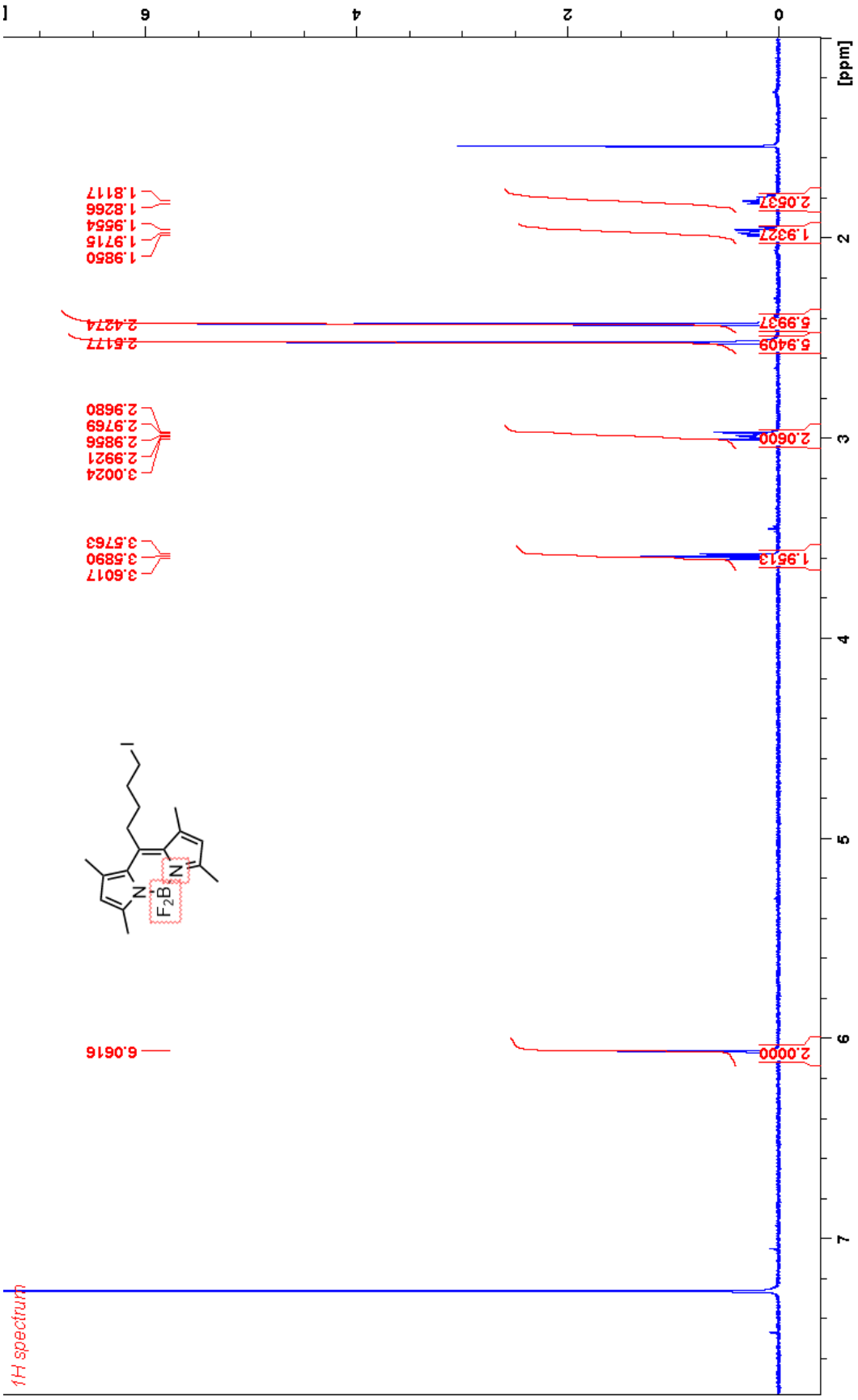
1H spectrum
[ppm]
6.0616
2.0000
2.0600
1.9513
3.0024
2.9921
2.9856
2.9769
2.9680
3.6017
3.5890
3.5763
2.4274
2.4177
5.9937
5.9409
2.0537
1.9327
1.9850
1.9715
1.9554
1.8266
1.8117
F2B
N
N

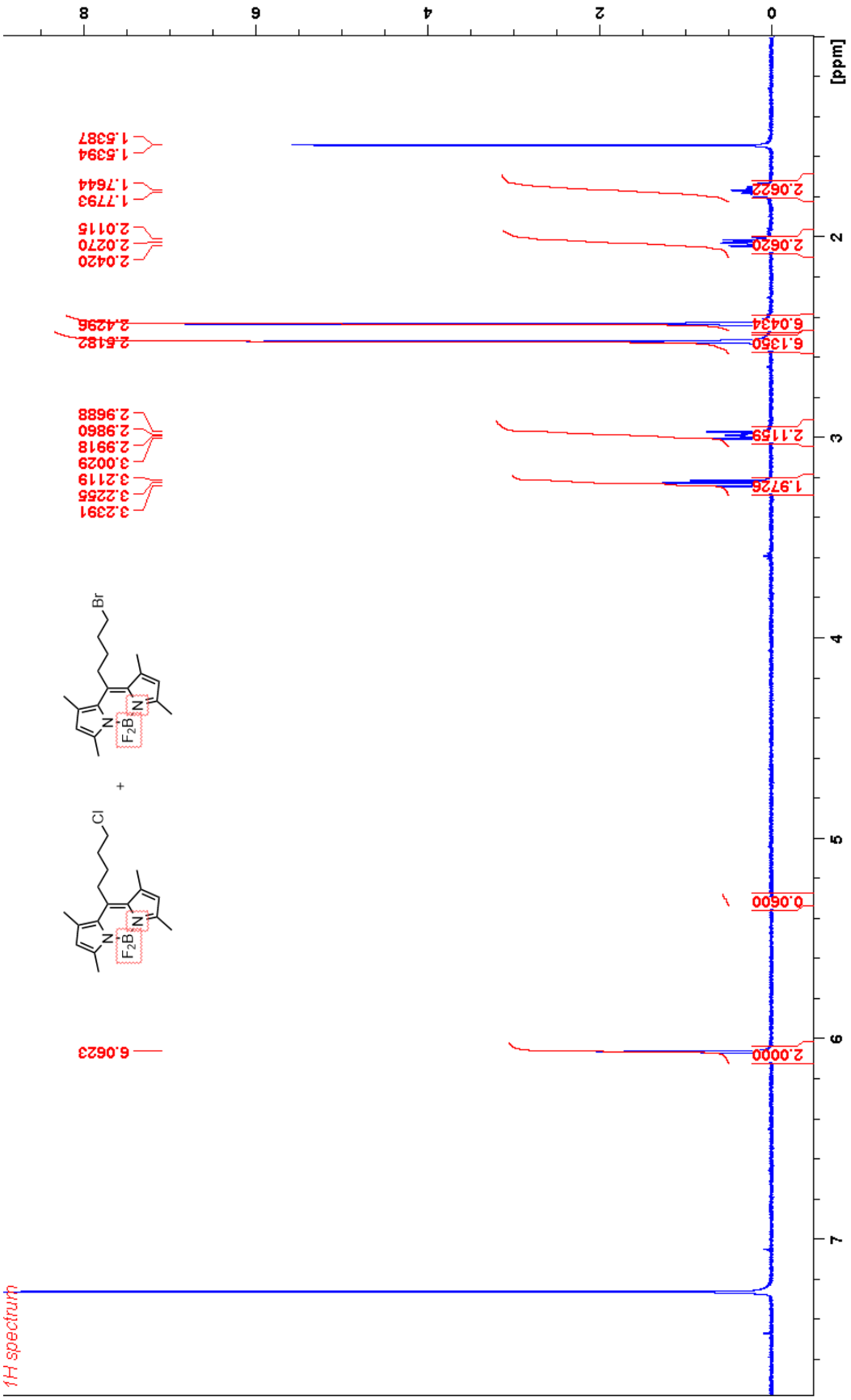
1H spectrum
[ppm]
0
2
4
6
8
1.5387
1.5394
1.7644
1.7793
2.0115
2.0270
2.0420
2.4296
2.4182
2.9688
2.9860
2.9918
3.0029
3.2119
3.2255
3.2391
6.0623
2.0000
0.0600
1.9726
2.1159
6.0434
6.1350
2.0620
2.0622
Br
Cl
F2B
N
+